ADVANCED MATERIALS
www.advmat.de

Planar $CH_3NH_3PbBr_3$ Hybrid Solar Cells with 10.4% Power Conversion Efficiency, Fabricated by Controlled Crystallization in the Spin-Coating Process

*Jin Hyuck Heo, Dae Ho Song, and Sang Hyuk Im**

Solar energy has been considered as a promising renewable and sustainable energy source because it is abundant enough to supply the energy demands of human beings on the earth. However, solar light is only available during the day so solar cells cannot generate electricity at night. In an effort to exploit solar energy all day long, many recent studies have been done to convert solar energy into chemical energy such as solar fuels. H_2 is the simplest product of solar fuel that can be directly produced from water-electrolysis by applying >1.23 V of potential or photo-catalytic water-splitting systems.[1] A prerequisite for this strategy is to develop cost-effective and highly efficient solar cells in order to cheaply produce the solar fuels from solar cells. Besides the importance of short-circuit current density (J_{sc}) to attain high power conversion efficiency of solar cells, it is still challenging to attain high open-circuit voltage (V_{oc}) in single-junction solar cells because over-potentials are generally required to generate solar fuels by electrolysis; such high open-circuit voltage solar cells can be used as the top cell in tandem solar cells.

Since Kojima et al.[2] reported a solution-processible organic–inorganic hybrid perovskite-sensitized solar cells using a liquid electrolyte and $CH_3NH_3PbX_3$ ($MAPbX_3$, X = Br, I), together with I^-/I_3^- as a sensitizer, perovskite solar cells based on solid-state halides[3] or mixed halides[4] have been demonstrated. To date, a power conversion efficiency of over 16% has been achieved for $CH_3NH_3PbI_3$ perovskite hybrid solar cells at 1 sun condition.[5]

Edri et al. reported on 1.3 V mesoscopic alumina/$MAPbBr_3$/N,N′-dialkyl perylenediimide (PDI) solar cells, but the efficiency was below 1%.[6] Qiu and co-workers attained 3.04% power conversion efficiency and V_{oc} of 1.16 V in mesoscopic TiO_2/$MAPbBr_3$/poly[N-9-hepta-decanyl-2,7-carbazole-*alt*-3,6-bis-(thiophen-5-yl)-2,5-dioctyl-2,5-di-hydropyrrolo[3,4-]pyrrole-1,4-dione] (PCBTDPP) solar cells.[7] Very recently, Ryu et al. reported a 6.7% efficiency and V_{oc} of 1.4 V in mesoscopic TiO_2/$MAPbBr_3$/poly-indenofluoren-8-triarylamine (PIF8-TAA).[8] However, the device efficiencies of $MAPbBr_3$ perovskite solar cells are not high enough for use in the production of solar fuel or as top cells for tandem devices. This may be attributed to the factor that deposition of dense $MAPbBr_3$ thin-films was not optimized because the probability of recombination between the electron conductor and hole conductor can be greatly suppressed by a pinhole-free $MAPbBr_3$ light absorbing interlayer. Here, we report the formation method for dense $MAPbBr_3$ thin-films on a blocking TiO_2 (bl-TiO_2)/FTO (F-doped SnO_2) substrate through controlling the crystallization process of $MAPbBr_3$ perovskite by inclusion of HBr solvent in $MAPbBr_3$/N,N-dimethylformamide (DMF) during single-step spin-coating. Due to this formation technique for dense $MAPbBr_3$ perovskite thin-films, we were able to fabricate planar $MAPbBr_3$ perovskite solar cells with the highest power conversion efficiency (10.4% at 1 sun condition) ever reported in $MAPbBr_3$ perovskite solar cells.

Figure 1 is a schematic illustration of the typical stages of the spin-coating process depicting what is happening in each stage. For a typical spin-coating process, we first dropped $MAPbBr_3$ solution on a bl-TiO_2/FTO substrate and accelerated the substrate to a certain rpm (revolutions per minute). During the acceleration, the excess solution is spun-off and the $MAPbBr_3$ solution is gradually dried by further evaporation of solvents inducing the crystallization of $MAPbBr_3$ perovskite. If we assume that the $MAPbBr_3$ solution behaves in a Newtonian fashion, the wet-thickness of the film h [m] with spinning time t [s] can be written as:[9,10]

$$\frac{dh}{dt} = -\frac{2\rho\omega^2}{3\eta}h^3 - \phi \quad (1)$$

where ω = radial velocity (rad s^{-1}), ρ = density (kg m^{-3}) of solution, η = viscosity (kg m^{-1} s^{-1}) of solution, and ϕ = evaporation rate (m s^{-1}). If we assume ϕ is independent on the size of the bl-TiO_2/FTO substrate and spinning time in the drying stage, it can be written as:[9,10]

$$\phi = k_g(C_v^i - C_v^0) \quad (2)$$

where C_v^i and C_v^0 are the concentration of solvent at the interface and in the bulk of vapor phase, respectively, and k_g is the mass transfer coefficient. Here, the driving force for evaporation of solvents is the vapor pressure, resulting in mass transfer of the solvents to air. As the radial distance increases from the rotating axis, forced convention becomes stronger due to the increased movement of the $MAPbBr_3$ wet-film in the angular direction so that ϕ will gradually increase along the radial distance. Practically, fresh laminar air-flow is sufficiently supplied onto the surface of the $MAPbBr_3$ wet-film so that ϕ will slightly increase along the radial distance. When the excess $MAPbBr_3$

J. H. Heo, D. H. Song, Prof. S. H. Im
Functional Crystallization Center (FCC)
Department of Chemical Engineering
Kyung Hee University
1732 Deogyeong-daero, Giheung-gu, Yongin-si
Gyeonggi-do 446–701, Republic of Korea
E-mail: imromy@khu.ac.kr

DOI: 10.1002/adma.201403140

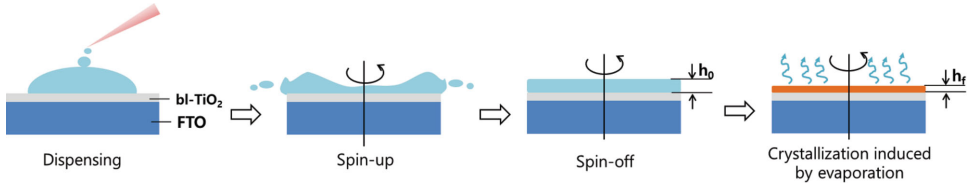

Figure 1. Schematic illustration of typical stage of spin-coating process (h_0 = thickness of wet film and h_f = thickness of dried film).

solution is spun-off by centrifugal force, the wet-thickness of the $MAPbBr_3$ solution on the bl-TiO_2/FTO substrate will reach a constant thickness of h_o, and the solid $MAPbBr_3$ perovskite thin-film with a final thickness (h_f) will form by further evaporation of residual solvents. Therefore, $h_0 \approx (3\eta\phi/2\rho\omega^2)^{1/3}$ stays about the same along the radial distance.

Here, it should be noted that the final film thickness (h_f) is greatly dependent on the solidification of the $MAPbBr_3$ solution during the crystallization process. To attain high device performance in planar $MAPbBr_3$ perovskite solar cells, it is crucial to form a dense $MAPbBr_3$ thin-film on the bl-TiO_2/FTO substrate. Accordingly, control of the crystallization process is critical to forming dense $MAPbBr_3$ films. Generally, the crystallization process consists of nucleation and growth stages, wherein nucleation depends on the supersaturation status (C^*), as shown in **Figure 2**a. The way to attain dense thin-films of $MAPbBr_3$ by using the same concentration of $MAPbBr_3$ solution is to reduce the evaporation rate of solvent or to increase the solvent solubility. The former requires significantly longer processing time to retard evaporation rate of solvent, so that it is not desirable for device fabrication. On the other hand, the latter is more desirable to reproducibly form dense thin-films because the concentration for supersaturation

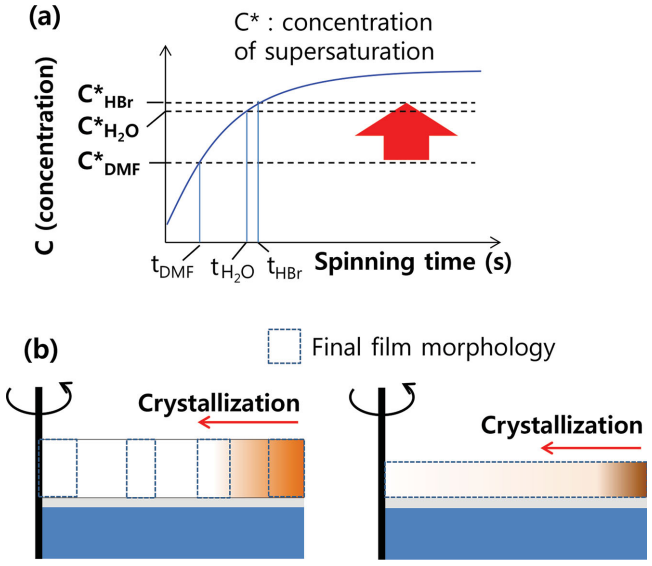

Figure 2. Schematic illustration for crystallization process during spin-coating. a) Crystallization behavior of the relation between concentration and spinning time: C^* = concentration of supersaturation, t = onset nucleation time; and b) onset crystallization with $MAPbBr_3$ solution with different solubility by spin-coating (dotted rectangle = the morphology of fully dried $MAPbBr_3$ film, the total area of dotted rectangles in left and right figure is similar)

(C^*) is increased, which initiates the nucleation process at higher concentrations of $MAPbBr_3$ wet films. If we assume that the evaporation rates of solvents are similar, the initial wet-film thickness (h_0) of $MAPbBr_3$ is same, and the final film-thickness (h_f) is determined by the concentration where crystallization begins in drying $MAPbBr_3$ wet films via further evaporation of solvent. Namely, crystallization in solution with higher solubility is initiated at a higher onset concentration. Therefore, a more concentrated $MAPbBr_3$ solution will form a thinner, dense $MAPbBr_3$ perovskite crystal layer on a bl-TiO_2/FTO substrate with more surface coverage. Figure 2b depicts a schematic illustration of the crystallization process of $MAPbBr_3$ films with a solubility difference. The crystallization (nucleation) is initiated from the edge of the $MAPbBr_3$ wet-film due to the highest evaporation rate of solvent and is propagated inward by further evaporation of solvent. A similar crystallization process occurred in the more soluble solution, but the onset time for crystallization will be delayed. Consequently h_f will be thinner due to more evaporated solvent, and the more concentrated solution results in a dense crystalline film with more surface coverage.

In order to check our concept, we prepared 40 wt% $MAPbBr_3$ in DMF, DMF+H_2O, and DMF+HBr solvent where 100 µL of H_2O and 48% HBr aqueous solvent was added in 1 mL of DMF solvent. The physical properties and crystallization time of each solution are summarized in **Table 1**. The order of boiling point (b.p.) of each solvent is H_2O (100 °C) < HBr (107.5 °C) < DMF (154 °C) under 1 atm, while the order for vapor pressure (v.p.) is DMF (0.52 kPa) < HBr (1.3 kPa) < H_2O (2.3 kPa) at 20 °C. Therefore, the order of evaporation rate (ϕ) of solvent is DMF < HBr < H_2O, however, the evaporation rate of the solution mixture will be similar because the main solvent is DMF in all three solutions. The order of solubility of $MAPbBr_3$ ionic compound in each solvent is DMF < H_2O < HBr. Hence, it is expected that the surface coverage of $MAPbBr_3$ thin-films will increase in the order of DMF < H_2O < HBr. **Figure 3** shows SEM surface and cross-sectional images of $MAPbBr_3$ films deposited on a bl-TiO_2/FTO substrate. As expected from the

Table 1. Physical properties of each solvent and crystallization characteristics of each $MAPbBr_3$ solution.

Physical properties	DMF	H_2O	HBr
Boiling point [°C] at 1 atm	154	100	107.5
Vapor pressure [kPa] at 20 °C	0.52	2.3	1.3
Crystallization characteristics of $MAPbBr_3$ solution	DMF	DMF + H_2O	DMF + HBr
Onset crystallization time [s]	40	80	93
Finished crystallization time [s]	48	100	115

Adv. Mater. **2014**,
DOI: 10.1002/adma.201403140

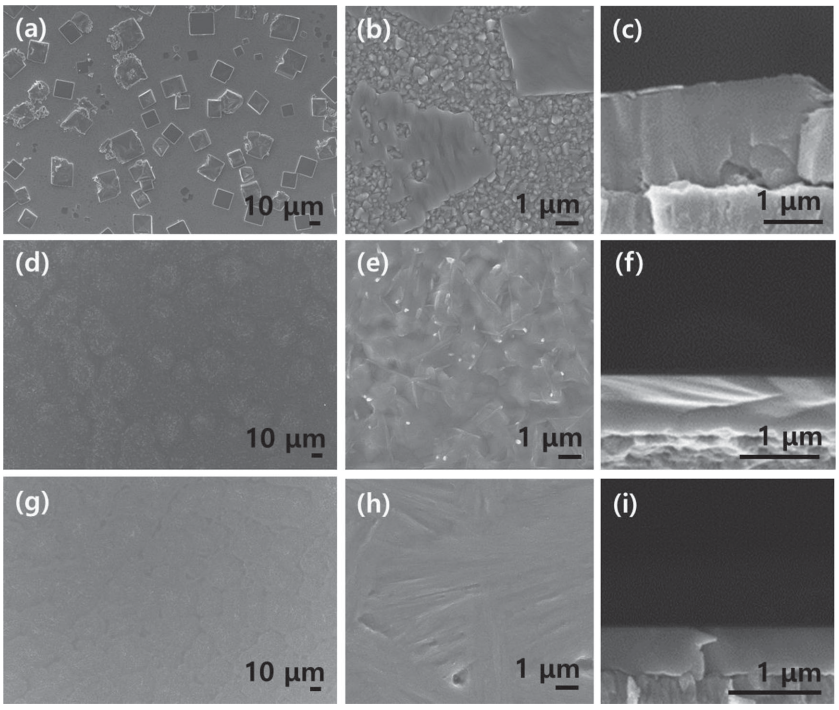

Figure 3. SEM surface and cross-sectional images of $MAPbBr_3$ perovskite thin-film deposited on bl-TiO_2/FTO substrate by the single-step spin-coating process with solutions with different solubility. a–c) DMF, d–f) DMF+H_2O, and g–i) DMF+HBr:DMF = 40 wt% $MAPbBr_3$ in 1 mL of DMF, DMF+H_2O = 40 wt% $MAPbBr_3$ in 1 mL of DMF + 0.1 mL of H_2O, DMF+HBr = 40 wt% $MAPbBr_3$ in 1 mL of DMF + 0.1 mL of HBr.

physical properties of the solvents, the $MAPbBr_3$/DMF solution formed isolated crystalline layers ca. 2 μm in thickness on a bl-TiO_2/FTO substrate while exposing uncoated parts as shown in Figure 3a–c. Meanwhile, the $MAPbBr_3$/DMF+H_2O and $MAPbBr_3$/DMF+HBr solutions made dense thin-films of ca. 0.8 μm-thickness, and ca. 0.5 μm-thickness, respectively (see Figure 3d–i). During the spin-coating process at 3000 rpm for 200 s, the $MAPbBr_3$/DMF solution was crystallized from the edge at ca. 40 s and was fully dried at ca. 48 s. The $MAPbBr_3$/DMF+H_2O and $MAPbBr_3$/DMF+HBr solutions were at ca. 80 s and ca. 100 s for nucleation and at ca. 93 s and ca. 115 s for full drying, respectively. Assuming that the evaporation rate of each solvent is similar, the amount of evaporated solvent is 2- and 2.3-fold higher in $MAPbBr_3$/DMF+H_2O and $MAPbBr_3$/DMF+HBr solutions relative to the $MAPbBr_3$/DMF solution. To calculate the surface coverage of $MAPbBr_3$ on bl-TiO_2/FTO substrate by spin-coating the $MAPbBr_3$/DMF solution, we checked the surface SEM images at the center, middle, and edge points as shown in Figure S1 in the Supporting Information. The surface coverage of the $MAPbBr_3$ layer was ca. 50% because the surface coverage at the center, middle, and edges were ca. 80%, 40%, and 30%, respectively. The final film-thicknesses (h_f) formed by $MAPbBr_3$/DMF, $MAPbBr_3$/DMF+H_2O, and $MAPbBr_3$/DMF+HBr were ca. 2, 0.8, 0.5 μm, respectively, so that the surface coverage of $MAPbBr_3$ films from $MAPbBr_3$/DMF+H_2O and $MAPbBr_3$/DMF+HBr solutions was 100% because the mass of $MAPbBr_3$ is conserved during the evaporation process in the final drying stage. These results are consistent with the crystallization process in Figure 2a because the $MAPbBr_3$/DMF solution forms more nuclei, causing rapid crystallization (solidification) of the solution due to the lowest C^* value originating from the lowest solubility. As a result, isolated, thick $MAPbBr_3$ layers are formed on the bl-TiO_2/FTO substrate.

To check if the dense $MAPbBr_3$ thin-film with full surface coverage enhances the device performance, we measured photocurrent density-voltage (J–V) curves of planar $MAPbBr_3$ perovskite solar cells composed of FTO/bl-TiO_2/$MAPbBr_3$/poly(3-hexylthiophene) (P3HT)/Au as shown in **Figure 4**a. The $MAPbBr_3$ solar cell prepared from $MAPbBr_3$/DMF solution exhibited the worst device performance (J_{sc} = 2 mA/cm^2, V_{oc} = 0.56 V, FF (fill factor) = 38%, and Eff. (efficiency) = 0.4%). The efficiency was greatly enhanced to 6.3% and 7.3% at 1 sun condition in solar cells prepared by $MAPbBr_3$/DMF+H_2O and $MAPbBr_3$/DMF+HBr solutions (see Table S1 in the Supporting Information). This result is associated with the fact that the $MAPbBr_3$ film with full surface coverage can greatly suppress the recombination of electrons and holes. Meanwhile, the $MAPbBr_3$ film with exposed bare bl-TiO_2 has significant recombination by direct contact of electron conductors and hole conductors. To understand why the $MAPbBr_3$/DMF+HBr solution provides better device performance than the $MAPbBr_3$/DMF+H_2O solution, we obtained XRD (X-ray diffraction) patterns, as shown in Figure 4b. The $MAPbBr_3$ perovskite prepared from the $MAPbBr_3$/DMF+H_2O solution revealed $PbBr_2$ and MABr peaks due to the decomposition of $MAPbBr_3$ by reaction with H_2O whereas the others are not. Here the $MAPbBr_3$ perovskite crystals were prepared by drying 1 mL of $MAPbBr_3$/DMF, $MAPbBr_3$/DMF+H_2O, and $MAPbBr_3$/DMF+HBr at 100 °C.

It is a well-known phenomenon that the perovskite solar cells exhibited large hysteresis of power conversion efficiency with forward and reverse bias scans because perovskite materials can accumulate the charge carriers[11] if the charges are not quickly transferred or transported into electron and hole conductors. Hence, the power conversion efficiency will be correct when the efficiency of the forward the scan coincides with the reverse scan result. Figure S2a in the Supporting Information shows the photocurrent-density–voltage (J–V) curves of a planar $MAPbBr_3$ solar cell prepared by $MAPbBr_3$/DMF+HBr solution (see Figure 4a) with a forward and reverse bias scan (delay time = 200 ms). This clearly shows that the J–V curves of forward and reverse scans are well matched. This might be attributed to quick separation and transport of charge carriers into the bl-TiO_2/$MAPbBr_3$/P3HT interface and bulk. This implies that a mesoporous TiO_2 layer is not necessary to remove the significant hysteresis of power conversion efficiency observed with scan direction in $MAPbBr_3$ perovskite solar cells if the charge carriers generated by the $MAPbBr_3$ light absorber

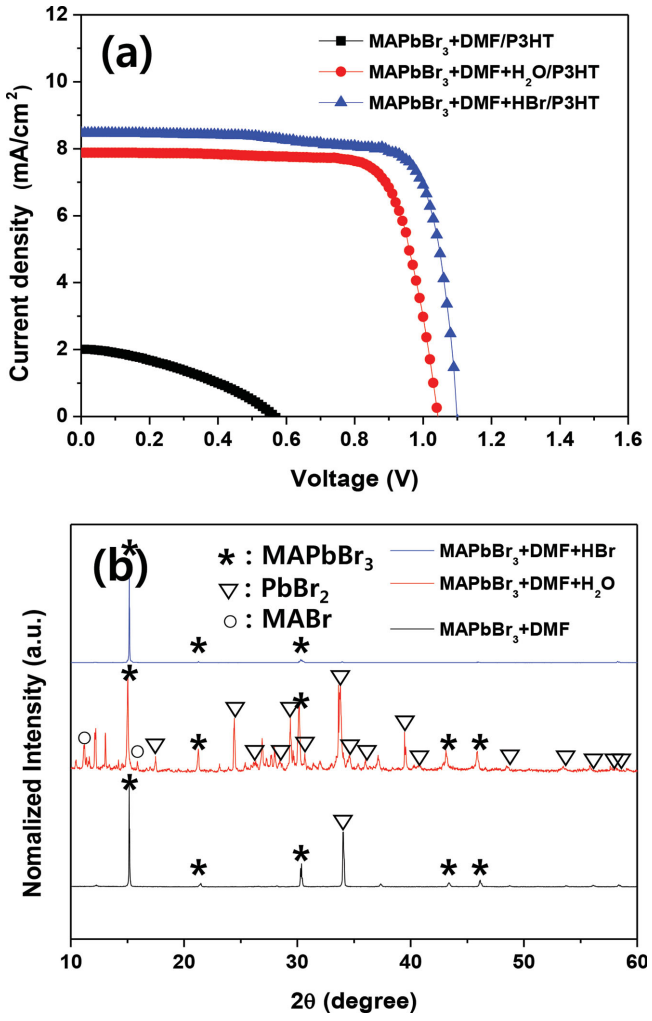

Figure 4. a) Photocurrent-density–voltage (*J*–*V*) curves of planar $MAPbBr_3$ perovskite solar cells with P3HT hole conductor where the $MAPbBr_3$ thin-films are prepared by solutions with different solubility. b) X-ray diffraction (XRD) patterns of $MAPbBr_3$ perovskite crystals prepared by drying 1 mL of $MAPbBr_3$/DMF, $MAPbBr_3$/DMF+H_2O, and $MAPbBr_3$/DMF+HBr at 100 °C.

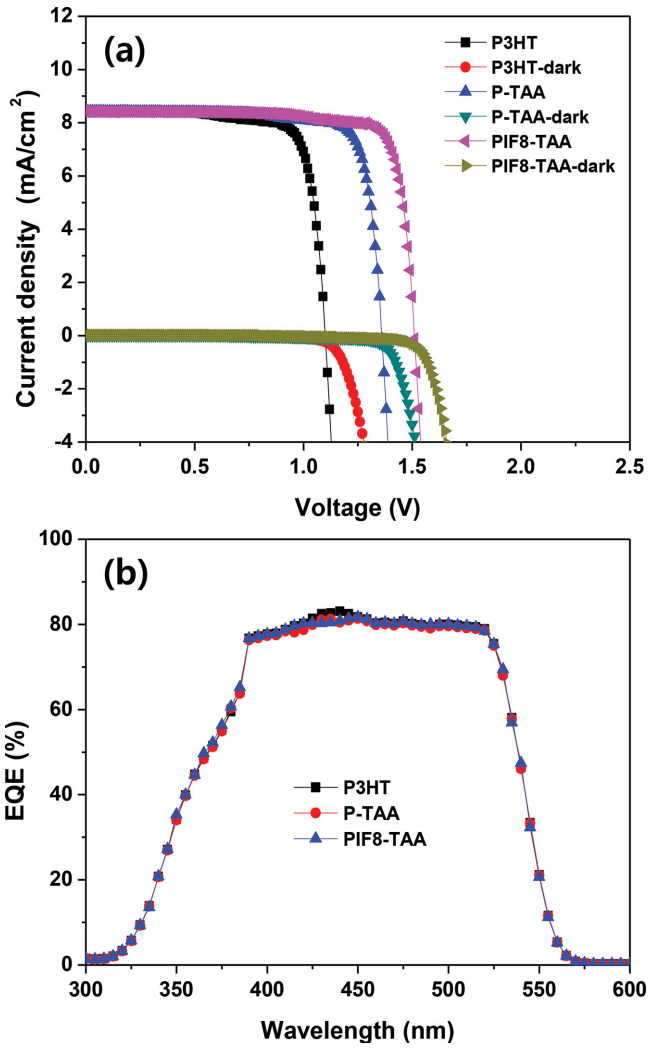

Figure 5. a) Photocurrent-density–voltage (*J*–*V*) curves and b) external quantum efficiency (EQE) spectra of planar $MAPbBr_3$ perovskite solar cells with different hole conductor.

are effectively transported within the $MAPbBr_3$ layer and both bl-TiO_2 and P3HT layers. This might be because the $MAPbBr_3$ has a longer diffusion length and better mobility of charge carriers than $MAPbI_3$ perovskite because the FF of planar $MAPbBr_3$ solar cells was high (79%) even though the thickness of the $MAPbBr_3$ layer is ca. 500 nm. The external quantum efficiency (EQE) spectrum of the planar $MAPbBr_3$ solar cell in Figure S2b in the Supporting Information shows that the EQE reaches ca. 80%.

To increase the open-circuit voltage (V_{oc}) of the planar $MAPbBr_3$ solar cells, we switched P3HT with poly(triarylamine) (P-TAA) and PIF8-TAA, because the highest occupied molecular orbital (HOMO) of P-TAA (–5.14 eV) and PIF8-TAA (–5.51 eV) are below that of P3HT (–5.0 eV).[8,12] **Figure 5**a shows the *J*–*V* curves of planar $MAPbBr_3$ perovskite solar cells with P3HT, P-TAA, and PIF8-TAA hole conductors under a forward scan direction with 200 ms delay time because not all samples showed hysteresis. With lowering of the HOMO of hole conductor, the V_{oc} was gradually increased in the order of P3HT (1.09 V) < P-TAA (1.35 V) < PIF8-TAA (1.51 V) as listed in **Table 2**. Therefore the overall power conversion efficiency was also gradually increased from 7.3% to 9.3% and to 10.4% at 1 sun illumination. To the best of our knowledge, this is the highest power conversion efficiency in $MAPbBr_3$ perovskite solar cells ever reported up to now. The tendency of increasing V_{oc} with the HOMO of hole conductors agreed

Table 2. Summary of device performance in planar $MAPbBr_3$ perovskite solar cells with different hole conductor.

Device	V_{oc} [V]	J_{sc} [mA/cm^2]	FF [%]	Eff. [%]
P3HT	1.09	8.5	79	7.3
P-TAA	1.35	8.4	82	9.3
PIF8-TAA	1.51	8.4	82	10.4

Adv. Mater. **2014**,
DOI: 10.1002/adma.201403140

well with the previously reported results in the literature.[3a,8] The high efficiency of planar $MAPbBr_3$ perovskite solar cells is attributed to the formation of a pure, dense $MAPbBr_3$ thin-layer on bl-TiO_2/FTO substrate by inclusion of HBr solvent during a single-step spin-coating process and replacement of P3HT with PIF8-TAA, which had a lower HOMO.

In summary, we deposited dense $MAPbBr_3$ perovskite thin-films with full surface coverage on a bl-TiO_2/FTO substrate by inclusion of HBr aqueous solution in a $MAPbBr_3$/DMF solution because the $MAPbBr_3$ in DMF+HBr solution retarded the nucleation time during the spin-coating process due to the better solubility than $MAPbBr_3$ in DMF solution. As a result, more-concentrated $MAPbBr_3$ in DMF+HBr solution yielded a thinner $MAPbBr_3$ perovskite layer with higher surface coverage. The inclusion of the same amount of H_2O instead of the HBr aqueous solvent also enables the formation of an $MAPbBr_3$ layer with full surface coverage on a bl-TiO_2/FTO substrate. However, the H_2O decomposed $MAPbBr_3$ into MABr and $PbBr_2$. Accordingly planar $MAPbBr_3$ perovskite solar cells prepared by $MAPbBr_3$ in a DMF+HBr solution exhibited the highest device efficiency of 7.3% at 1 sun condition. By switching the P3HT hole conductor with P-TAA and PIF8-TAA, the overall power conversion efficiency was gradually enhanced to 9.3% and 10.4%, respectively, at 1 sun illumination, due to the lowered HOMO level. In addition, the planar $MAPbBr_3$ perovskite solar cells did not have significant hysteresis of power conversion efficiency with scan direction, possibly due to efficient charge separation and transport in the bulk and at the interface of bl-TiO_2/$MAPbBr_3$/P3HT. We believe that the perovskite solar cells with high open-circuit voltage can be applicable to efficient water-splitting system.

Experimental Section

Preparation of $CH_3NH_3PbBr_3$ Perovskite Solution: CH_3NH_3Br was synthesized by reacting 50 mL of hydrobromic acid (48% in water, Aldrich) and 30 mL of methylamine (40% in methanol, Junsei Chemical Co. Ltd.) in a 250-mL round-bottom flask at 0 °C for 2 h with stirring. The precipitates were recovered by evaporation at 50 °C for 1 h. The products were dissolved in ethanol, recrystallized from diethyl ether, and finally dried at room temperature in a vacuum oven for 24 h. 40 wt% $CH_3NH_3PbBr_3$ solution was prepared by reacting the synthesized CH_3NH_3Br powder and $PbBr_2$ (Aldrich) at 1:1 mole ratio in DMF at 60 °C for 30 min.

Device Fabrication: To prepare the mesoscopic TiO_2 film, a dense TiO_2 blocking layer (bl-TiO_2) of ca. 50-nm thickness was deposited on cleaned F-doped SnO_2 (FTO) (Pilkington, TEC8) glass substrate by spray-pyrolysis deposition (SPD) method with 20 mM of titanium diisopropoxide bis(acetylacetonate) (Aldrich) solution at 450 °C. To form the $CH_3NH_3PbBr_3$ layer on bl-TiO_2/FTO substrate, the 40 wt% $CH_3NH_3PbBr_3$/DMF solution with an added 100 μL of HBr was then coated by spin-coating at 3000 rpm for 200 s and dried on a hot plate at 100 °C for 2 min. Poly(3-hexylthiophene) (P3HT) (Lumtec) hole-transporting materials (HTMs) were spin-coated on $CH_3NH_3PbBr_3$/bl-TiO_2/FTO substrate at 3000 rpm for 30 s by using HTM/toluene (15 mg/1 mL) both with 7.5 μL of Li-bis(trifluoromethanesulfonyl) imide (Li-TFSI)/acetonitrile (170 mg/1 mL) and 7.5 μL of t-BP/acetonitrile (1 mL/1 mL) additives and without additives. Finally, a Au counter electrode was deposited by thermal evaporation. The active area was fixed to 0.16 cm^2. All the device fabrications were conducted below 50% of relative humidity.

Device Characterization: The external quantum efficiency (EQE) was measured using a power source (ABET 150 W Xenon lamp, 13014) with a monochromator (DONGWOO OPTORN Co., Ltd., MonoRa-500i) and a potentiostat (IVIUM, IviumStat). The current-density–voltage (*J–V*) curves were measured using a solar simulator (Peccell, PEC-L01) with a potentiostat (IVIUM, IviumStat) at 100 mA cm^{-2} illumination AM 1.5G and a calibrated Si-reference cell certificated by JIS (Japanese Industrial Standards). For the measurement of the hysteresis of the *J–V* curves, the forward and reverse scan rates were both set to 200 ms/10 mV. The *J–V* curves of all the devices were measured by masking the active area with metal mask of 0.096 cm^2.

Supporting Information

Supporting Information is available from the Wiley Online Library or from the author.

Acknowledgements

This study was supported by Mid-career Research Program (No.:NRF-2013R1A2A2A01067999) and Basic Science Research Program (No. 2014R1A5A1009799) through the National Research Foundation of Korea (NRF) funded by the Ministry of Science, ICT & Future Planning.

Received: July 14, 2014
Revised: September 25, 2014
Published online:

[1] M. G. Walter, E. L. Warren, J. R. McKone, S. W. Boettcher, Q. Mi, E. A. Santori, N. S. Lewis, *Chem. Rev.* **2010**, *110*, 6446.
[2] A. Kojima, K. Teshima, Y. Shirai, T. Miyasaka, *J. Am. Chem. Soc.* **2009**, *131*, 6050.
[3] a) J. H. Heo, S. H. Im, J. H. Noh, T. N. Mandal, C.-S. Lim, J. A. Chang, Y. H. Lee, H.-J. Kim, A. Sarkar, M. K. Nazeeruddin, M. Grätzel, M. S. I. Seok, *Nat. Photonics* **2013**, *7*, 486; b) H.-S. Kim, C.-R. Lee, J.-H. Im, K.-B. Lee, T. Moehl, A. Marchioro, S.-J. Moon, R. Humphry-Baker, J.-H. Yum, J. E. Moser, M. Grätzel, N.-G. Park, *Sci. Rep.* **2012**, *2*, 591; c) J. Burschka, N. Pellet, S.-J. Moon, R. Humphry-Baker, P. Gao, M. K. Nazeeruddin, M. Grätzel, *Nature* **2013**, *499*, 316; d) J. H. Noh, S. H. Im, J. H. Heo, T. N. Mandal, S. I. Seok, *Nano Lett.* **2013**, *13*, 1764; e) D. Liu, T. L. Kelly, *Nat. Photonics* **2014**, *8*, 133; f) H.-S. Kim, S. H. Im, N.-G. Park, *J. Phys. Chem. C* **2014**, *118*, 5615.
[4] a) M. M. Lee, J. Teuscher, T. Miyasaka, T. N. Murakami, H. J. Snaith, *Science* **2012**, *338*, 643; b) M. Liu, M. B. Johnston, H. J. Snaith, *Nature* **2013**, *501*, 395.
[5] N. J. Jeon, H. G. Lee, Y. C. Kim, J. Seo, J. H. Noh, J. Lee, S. I. Seok, *J. Am. Chem. Soc.* **2014**, *136*, 7837.
[6] E. Edri, S. Kirmayer, D. Cahen, G. Hodes, *J. Phys. Chem. Lett.* **2013**, *4*, 897.
[7] B. Cai, Y. Xing, Z. Yang, W.-H. Zhang, J. Qiu, *Energy Environ. Sci.* **2013**, *6*, 1480.
[8] S. Ryu, J. H. Noh, N. J. Jeon, Y. C. Kim, W. S. Yang, J. Seo, S. I. Seok, *Energy Environ. Sci.* **2014**, *7*, 2614.
[9] R. M. van Hardeveld, P. L. J. Gunter, L. J. van IJzendoorn, W. Wieldraaijer, E. W. Kuipers, J. W. Niemantsverdriet, *Appl. Surf. Sci.* **1995**, *84*, 339.
[10] a) A. G. Emslie, F. T. Bonner, L. G. Peck, *J. Appl. Phys.* **1958**, *29*, 858; b) D. Meyerhofer, *J. Appl. Phys.* **1978**, *49*, 3993; c) C. J. Lawrence, *Phys. Fluids* **1988**, *31*, 2786.
[11] H. J. Snaith, A. Abate, J. M. Ball, G. E. Eperon, T. Leijtens, N. K. Noel, S. D. Stranks, J.T.-W. Wang, K. Wojciechowski, W. Zhang, *J. Phys. Chem. Lett.* **2014**, *5*, 1511.
[12] S. H. Im, C.-S. Lim, J. A. Chang, Y. H. Lee, N. Maiti, H.-j. Kim, M. K. Nazeeruddin, M. Grätzel, S. I. Seok, *Nano Lett.* **2011**, *12*, 4789.